



# Numerical and Experimental Analysis of a Solid Shroud in Multi-arc Plasma Spraying

K. Bobzin<sup>1</sup> · H. Heinemann<sup>1</sup> · A. Dokhanchi<sup>1</sup>

Submitted: 21 July 2023 / in revised form: 27 November 2023 / Accepted: 26 December 2023 / Published online: 12 February 2024  
© The Author(s) 2024

**Abstract** Plasma spraying is characterized by high flexibility, but has challenges of high energy consumption and oxidation of the metallic spray particles. Modified plasma spraying processes using a gas or solid shroud have been developed to address these challenges, which aim to reduce the introduction of ambient air into the plasma jet and improve the process efficiency. Prior research mainly focused on single-cathode plasma generators, and the use of a shroud in multi-arc plasma spraying systems has not been thoroughly explored. The primary goal of this study is to analyze the effects of a solid shroud as a nozzle extension on the plasma jet of a three-cathode plasma generator numerically and experimentally. Computational fluid dynamics (CFD) is used to simulate a solid shroud, and the resulting design is constructed for experimental analysis. The experimental setup includes a nozzle extension with a transparent window for diagnostic measurements by a high-speed camera. To isolate the effects of the solid shroud from fluctuations in the power input, current, and voltage measurements are carried out synchronized with the high-speed recordings. Particle diagnostics are also conducted to analyze the properties of the in-flight particles without and with the solid shroud. The developed numerical model can be further used to optimize the shroud geometry for different process parameters.

**Keywords** CFD simulation · diagnostic measurements · energy efficiency · plasma spraying · solid shroud

## Introduction

Plasma spraying is one of the most versatile variants of thermal spraying as a coating technology. In most cases, the required plasma is generated by a DC plasma generator, and the process takes place at atmospheric pressure. This process, called atmospheric plasma spraying (APS), is characterized by high flexibility, which is due to the wide range of thermal and kinetic energies of the spray particles (Ref 1). The APS process has gained significant attention due to its potential applications in various industries such as aerospace, automotive, and biomedical. However, its high energy consumption compared to other thermal spraying process variants and oxidation of the spray particles are significant challenges that need to be addressed. In APS, less than 5 % of the energy present in the plasma jet is utilized for the acceleration and melting of particles (Ref 2, 3). Considering an energy demand of 9–22 kWh per kilogram of molten powder particles, APS needs approximately twenty times more energy compared to wire arc spraying, which consumes between 0.2 and 0.4 kWh per kilogram of feedstock material (Ref 4). Additionally, in APS, a significant portion of the total input energy is utilized for cooling the electrodes. While the increased current contributes to effective power enhancement, the thermal efficiency is reduced as more electrical energy dissipates into the cooling water (Ref 5). In a prior study by the authors (Ref 6), the net power and cooling loss were examined for various combinations of process parameters using a three-cathode plasma generator. For example, in a scenario with 50 SLPM argon and 500 A electric current, the calculated cooling loss and net power were 19.8 and 27.3 kW, respectively, resulting in an efficiency of 56.3 % for the APS system (Ref 6). The low energy efficiency of APS is mainly because of air entrainments in the plasma jet. High velocity differences between

✉ A. Dokhanchi  
dokhanchi@iot.rwth-aachen.de

<sup>1</sup> Surface Engineering Institute (IOT), RWTH Aachen University, Aachen, Germany

the plasma jet and the surrounding fluid generate strong shear forces, resulting in the formation of cold air eddies at the nozzle exit. Downstream of the flow, these eddies dissolve and mix with the plasma gas that leads to rapid cooling of the plasma jet (Ref 7). The rate of cooling of the plasma is also dependent on the surrounding gas. Two-atom gases such as  $N_2$  and  $O_2$ , which are present in ambient air, require additional energy for dissociation, leading to a greater temperature reduction in the plasma jet compared to monoatomic gases such as argon or helium. The rapid mixing of plasma with surrounding gas induces changes in plasma composition, especially through the dissociations of oxygen molecule at about 3500 K and nitrogen molecule at about 7000 K. This leads to a faster cooling of the plasma jet for oxygen compared to nitrogen, due to the high energy consumption associated with these dissociation reactions (Ref 8). In view of the aforementioned phenomena, modified plasma spraying processes have been developed in addition to the conventional APS, which are shown in Fig. 1 and listed below:

- I. Plasma spraying within a chamber under vacuum or controlled atmosphere
- II. Gas shielding plasma spraying with a gaseous barrier
- III. Plasma spraying with a solid barrier
- IV. Gas shielding plasma spraying with both a gaseous and a solid barrier

These processes reduce the introduction of ambient air into the plasma jet and/or improve the efficiency of the plasma spraying process. The choice of process depends on the specific application and desired coating properties. The common feature of these modifications is the separation of the plasma jet from the surrounding atmosphere to achieve

a higher plasma temperature, which increases the molten ratio of the particles and additionally reduces the oxidation of the particles. The most technologically advanced equipment is required for vacuum plasma spraying or plasma spraying in a controlled atmosphere, but the oxide content achieved in this coating is the lowest among the different variants (Ref 9). Gas-shielded plasma spraying was established as an alternative to vacuum plasma spraying for the application of oxide-free MCrAlY coatings on turbine blades (Ref 10). The development of gas shroud systems as a nozzle attachment for plasma spraying has been a subject of interest in several research works available in the literature (Ref 11). Thomson et al. (Ref 12) conducted a study on the use of a gas shroud attachment for a plasma torch nozzle. Through the use of particle diagnostics, flow visualization, and coating characterization techniques, they were able to evaluate the performance of the attachment. They found that the shroud system resulted in an increase in coating density and adhesion. Planche et al. (Ref 13) explored the differences in coating oxidation and porosity for nitrogen and compressed air shrouding systems using a single-cathode plasma generator. Morks et al. (Ref 14) investigated the impact of nozzle type, termed as normal and high-speed nozzle, and gas shroud on the microstructure and properties of plasma-sprayed NiCr coatings on mild steel substrate. The results revealed that the use of a gas shroud system with a normal nozzle enhanced the coating corrosion resistance due to the formation of dense coatings. However, when a high-speed nozzle was used in combination with a shroud, the coating hardness decreased because of the increase in partially melted particles within the coatings.

The combination of the air entrainment process and the elevated temperatures experienced in the plasma jet causes

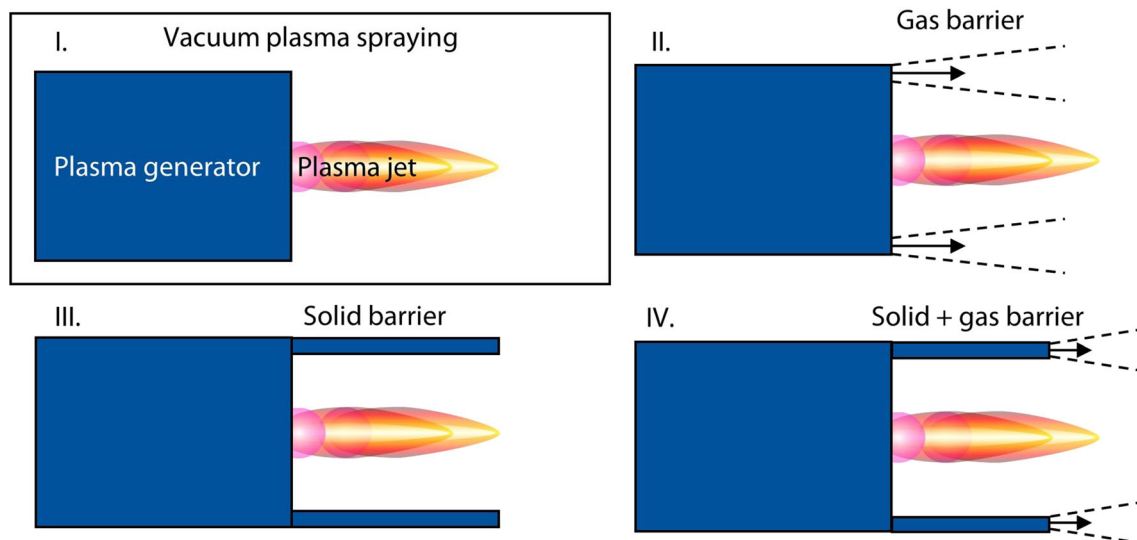


**Fig. 1** State-of-the-art for different shroud structures in plasma spraying

the oxidation of the injected metallic particles. The occurrence of these two oxidation stages leads to decreased mechanical properties, particularly in terms of coating ductility, and impairs the corrosion resistance of metallic coatings (Ref 15). The in-flight oxidation of particles alters their composition before impact on the substrate, subsequently modifying their melting properties. The effect of oxidation on iron particles during flight as well as upon deposition was investigated in a study by Espie et al. (Ref 15). They concluded that oxidation of metals and alloys cannot be eliminated in APS applications but can be reduced considerably by shrouding the plasma jet with a combustible gas such as acetylene. In another work by Espie et al. (Ref 16), the amount of oxidation was quantified experimentally using APS in a dc Ar-H<sub>2</sub> (50:10 SLPM) plasma jet. It was determined that the oxidation occurs not only on the surface but predominantly within the core of the particles, driven by intense convection within the droplets. This oxide phase (FeO) amounted about 12 wt.% of the collected particles. Furthermore, Zhang et al. (Ref 17) also investigated the in-flight oxidation of plasma-sprayed iron particles. They found that the majority of oxidation takes place in the liquid phase, and the thickness of the surface oxide layer, approximately 0.1 μm, is not significantly influenced by particle temperature and velocity before particle melting.

One advantage of using a solid shroud in plasma spraying is that it can help to prevent the interaction of air with the plasma. This is because a solid shroud creates a physical barrier between the plasma and the surrounding atmosphere, whereas a gas shroud relies on the use of an inert gas to displace the air and create a protective atmosphere. Furthermore, a solid shroud can be easier to use and maintain compared with a gas shroud, as it does not require the use of additional gases or complex control systems. This can help to reduce the overall complexity and cost of the plasma spraying process. Although the solid shield offers advantages, there are also practical challenges associated with it. One of the primary issues is that it is typically made of metal and requires cooling to keep it at a suitable temperature. The design of the geometry with respect to the allowable wall temperatures is a critical factor. Another challenge is that there is a tendency for molten particles to adhere to the internal wall of the shield, which can necessitate frequent cleaning and limit the effectiveness of the solution approach. Clogging due to completely molten particles can be prevented by adjusting appropriate geometric parameters for the shroud, such as the divergent angle and the length.

Liu et al. (Ref 18) investigated the impact of a solid shield structure on plasma spray processes and identified an optimal shield structure using simulations. They concluded that using a conical shield with a divergence angle of 5.5

degrees and a length of 90 mm is effective in forming a low-oxygen and high-temperature region in the plasma flame, resulting in higher particle temperature and fewer oxidized coatings. However, substrate overheating and velocity reduction may occur. According to a research work by Matthews (Ref 19), the oxidation mechanism in atmospheric plasma spraying process can be categorized into three types: solid-state oxidation of starting powder, in-flight oxidation, and post-impact oxidation on the substrate. The study found that using a solid shroud without shroud gas was helpful in minimizing in-flight oxidation, but it was not as effective in reducing layer to layer oxidation, when used at a short shroud-substrate separation distance of 10 mm. Kim et al. (Ref 20) explored the use of nitrogen gas shroud together with a solid shield to reduce oxidation and crystallization of bulk metallic glasses. The comparison between coatings prepared using the shroud system and common APS process was made by studying deposition behavior, oxidation and heat-induced crystallization mechanisms. They found that the shroud system could effectively control oxidation and crystallization, leading to better corrosion resistance properties and an increase in the amorphous fraction of the coating.

Overall, shielding the plasma jet is a promising approach to increase the energy efficiency of plasma spraying and improve coating properties. The plasma spraying variants I, II, and IV in Fig. 1 require either high technological effort to achieve separation of the plasma jet from the environment or additional resources due to the use of a gas shroud. The variant III, which separates the plasma jet with a solid barrier, presents a resource-efficient solution by eliminating the need for additional gas resources. While the basic functionality of this concept has already been demonstrated, targeted optimization of the shroud geometry can further increase the efficiency of the process. Research on developing new designs and optimizing the operation of shroud systems is limited in the literature. To achieve this objective, one possible initial step is to create a numerical model of the plasma jet with a nozzle extension using different parameters. This model would enable the examination of how various process parameters and nozzle extension geometries impact the plasma flow. A simplified numerical model based on energy conservation and wall functions was conducted by Gawne et al. (Ref 21) to predict the impact of a substrate, solid shield, and gas shroud on the plasma jet temperature and velocity profiles. They observed a significant decrease in the axial velocity of the plasma jet, as well as a notable increase in temperature in the radial direction. By comparing the solid shield and gas shroud, they determined that the solid shield can generate high flow temperatures but may be vulnerable to particle adhesion on its inner surface. On the other hand, the gas shroud does not have these drawbacks but may result in

lower flow temperatures and a less stable barrier that tends to dissipate downstream. In another numerical study, Janovic and Mostaghimi (Ref 22) created a 2D model of a curvilinear nozzle extension with gas mantle to investigate how parameters, such as the cone angle and main gas flow rate can influence the flow pattern inside the nozzle. They concluded that an adapted shape, which follows the streamlines of the fluid, further increases the plasma temperatures and velocities. Nonetheless, 2D simulations are limited in their ability to explore how plasma interacts with particles. They also tested their curvilinear nozzle design experimentally (Ref 23). It proved to be capable of withstanding high plasma temperatures and enabled satisfactory particle injection.

There is an optimal solid barrier geometry for each combination of process parameters and spray gun that minimizes the mixing of the plasma jet with the surrounding air. The possible lack of a commercially available shrouding system can also be attributed to this fact that shroud design is case-dependent. Wang et al. (Ref 24) expressed the challenges associated with the careful selection of a shroud length that strikes a good balance between optimizing the flow characteristics and minimizing air entrainment. They proposed a narrow gap between the downstream end of the cylindrical shield and the substrate surface, as a shorter solid shield may not significantly reduce ambient air entrainment. They noted that the suitable size of this gap for a turbulent plasma jet is considerably larger than that for a laminar one. In turbulent cases, overheating of the solid shield or substrate could pose a problem, necessitating additional cooling measures to completely prevent the entrainment of ambient air. In another study, Dolatabadi et al. (Ref 25) put forth the idea that optimizing the shroud geometry can help to minimize the large recirculating flow within the shroud, and thus improve particle velocities and temperatures. However, only a few simulation-based approaches have been conducted to optimize the geometry based on flow conditions and improve energy efficiency in plasma spraying. Furthermore, the majority of previous studies have used conventional single-cathode plasma generators and the use of a solid shroud in multi-arc plasma spraying systems has not been thoroughly investigated. Multi-arc spraying systems, together with new torch designs, promise to increase the achievable deposition efficiencies and enlarge the process window with respect to particle temperatures and velocities, compared to conventional single-arc systems (Ref 26). In a previous work by the authors (Ref 27) an initial CFD model for simulating a solid shroud for multi-arc plasma spraying was developed and the fundamental functionality of such a shroud in multi-arc plasma spraying was demonstrated. The current study aims to enhance this numerical model and to conduct experimental analysis of a

solid shroud utilized as a nozzle extension in multi-arc plasma spraying. To this end, computational fluid dynamics (CFD) approaches are used to model the plasma jet of a three-cathode plasma generator in the presence of a solid shroud with cooling channels while considering heat transfer phenomena. The simulated solid shroud was then constructed for experimental analysis of its effects on the plasma jet. The constructed nozzle extension has an inspection window closed with a transparent quartz glass for diagnostic measurements by a high-speed camera. Furthermore, the wall temperature of the nozzle extension was monitored by thermal sensors. The voltages between the cathodes and the anode of the plasma generator, as well as the current flowing there, are proportional to the power introduced into the plasma jet. To distinguish the influence of the solid shroud on the flow conditions in the plasma jet from the influence of fluctuations of the power input, synchronized (triggered) current, and voltage measurements are carried out with high-speed recordings. Furthermore, particle diagnostics are conducted experimentally to analyze the in-flight particle properties without and with the solid shroud. The developed parametrized model of the nozzle extension, together with the experimental measurements, can be further used to optimize the shroud geometry to adapt it to the flow conditions of the plasma jet for different process parameters.

## Numerical Modeling

This study utilizes CFD models of a multi-arc APS process that were previously developed at the Surface Engineering Institute (IOT) of RWTH Aachen University. The plasma spraying process of a three-cathode plasma generator was simulated numerically by modeling sub-processes individually and then coupling them together. This approach is used to simplify the overall process simulation and to better capture specific physical phenomena at different time and length scales. The plasma generator model and the plasma jet model, which include plasma–particle interactions, are the two sub-models that are particularly relevant to this study.

The plasma generator model was developed based on the three-cathode torch TriplexPro<sup>TM</sup>-210 from Oerlikon Metco in Wohlen, Switzerland. The model adopts the continuum approach and assumes that the plasma is in local thermodynamic and chemical equilibrium. This approach considers the overall plasma flow and does not examine local changes in electron and heavy ion properties. The three-cathode plasma generator possesses a three-fold axial symmetry allowing for one-third of the geometry to be used as the computational domain. This involves the incorporation of the electrodes within the calculation

domain, as depicted in Fig. 2. A two-equation Shear Stress Transport (SST) turbulence model was used to compute the turbulence within the plasma generator and plasma jet. The profiles of temperature, velocity, turbulent kinetic energy, and turbulent eddy dissipation were determined at the plasma generator outlet. The plasma jet model then incorporates this plasma flow profile data as input. Further details about the plasma generator model used in this work can be found in Ref 26, 28.

The two sub-models, plasma generator model and plasma jet model, were connected by using the calculated profiles of the plasma generator model at the nozzle exit as a boundary condition for the plasma jet model. To reduce computational cost, a steady-state approach was used in this study, employing the Reynolds-averaged Navier–Stokes (RANS) method to simulate turbulence in both the plasma generator and plasma jet models. The particles are introduced into the computational domain through an injection inlet with defined mass flow rate, initial velocity, and size distributions in spherical forms. For accurate representation of the interaction between plasma and particles during plasma spraying, the plasma jet model includes the effects of particles on the plasma velocity and temperature fields in a fully coupled manner. Therefore, the plasma jet model is capable of describing the particle trajectories and dependent changes in particle temperature, velocity, size, and thermophysical state, i.e., solid, liquid, and gas. Please refer to Ref 29 for further details regarding the plasma–particle interaction in the plasma jet model. An earlier study (Ref 28) conducted an experimental validation of both the plasma generator and plasma jet models.

In this study, the plasma jet model mentioned earlier is developed further to include a fixed solid shroud as a nozzle extension. Furthermore, the plasma generator model is used to calculate the profile data of the plasma flow for a set of process parameters directly at the nozzle exit. All simulations were performed using the commercial CFD

software package ANSYS CFX version 22.2, ANSYS Inc., Canonsburg, USA. To simulate the particle–plasma interaction, 2,000 particle trajectories were calculated. The simulations use aluminum oxide as a ceramic feedstock material with particle size distribution of  $-45 + 22 \mu\text{m}$ . This study focuses on the multi-arc plasma spraying of ceramic feedstock materials, with alumina chosen as an illustrative example due to its readily available material data in the literature. The specific heat capacity of this feedstock material is modeled as temperature and physical state-dependent using NASA polynomials (Ref 30). The enthalpies at melting and boiling temperatures are utilized to determine the values of latent heat of fusion and boiling. Enthalpy values are further computed using NASA polynomials. For simplification, a constant thermal conductivity of  $\kappa = 6 \text{ W/mK}$ , corresponding to higher temperatures, is applied in this work for the alumina feedstock material. The numerical model accounts for the trajectories of the particles, as well as associated variations in their temperature, velocity, size, and thermophysical state (solid, liquid, and gas).

Figure 3 shows the computational domain of the plasma jet with a nozzle extension. The technical drawing of the simulated nozzle extension is depicted in Fig. 4. The study considers a conical nozzle extension directly at the nozzle outlet of the plasma generator with a length of  $L = 100 \text{ mm}$ . To prevent any adverse impact of the pressurized air on the plasma flow and coating properties with respect to the particle oxidation, the outlets of the cooling channels are bent to the side.

The numerical model comprises two distinct domains: the solid domain, which encompasses the solid shroud, and the fluid domain containing a mixture of gases along with the initially solid-state injected aluminum oxide particles. To establish the interaction between these domains, a fluid–solid interface is defined at the boundary. The simulation enclosure allows for the analysis of heat transfer between

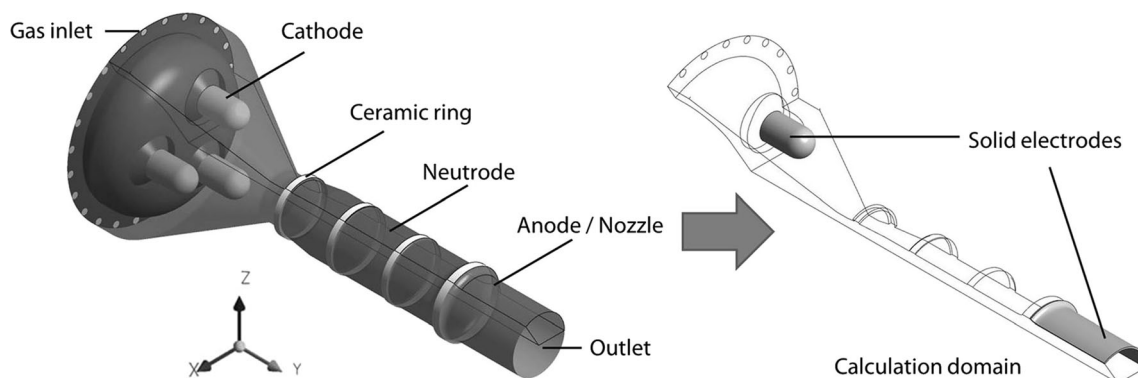


**Fig. 2** Interior geometry of the TriplexPro™-210 torch from Oerlikon Metco and calculation domain (Ref 26). Modeling Multi-Arc Spraying Systems, K. Bobzin and M. Öte, Journal of Thermal

Spray Technology, Vol. 25, Springer Nature, 2016, reproduced with permission from SNCSC.

**Fig. 3** Setup of the boundary conditions of the plasma jet model with nozzle extension

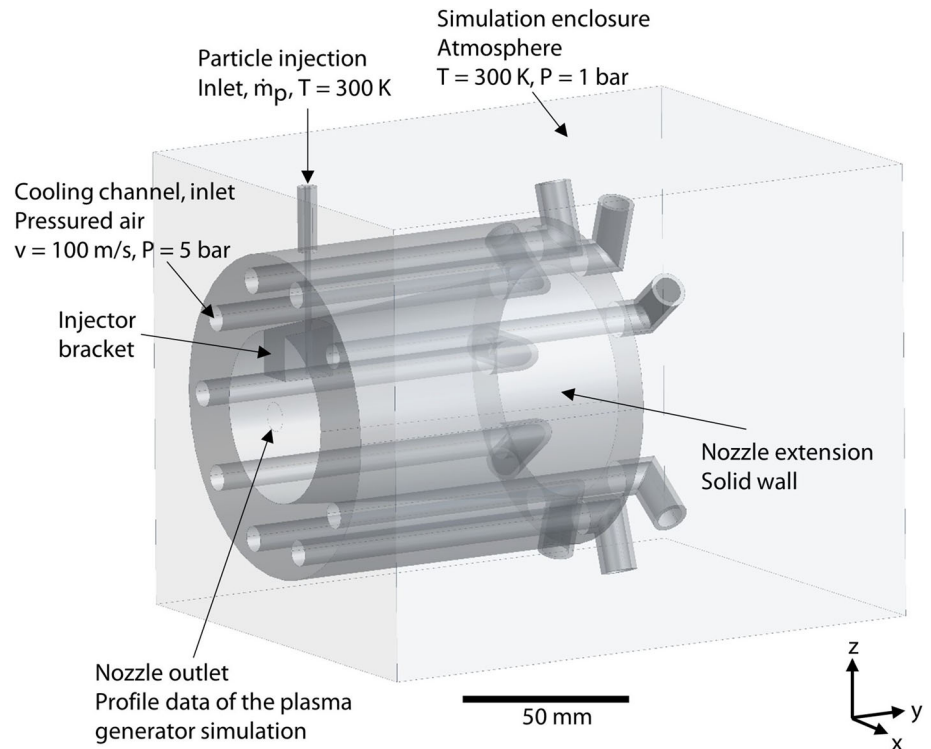
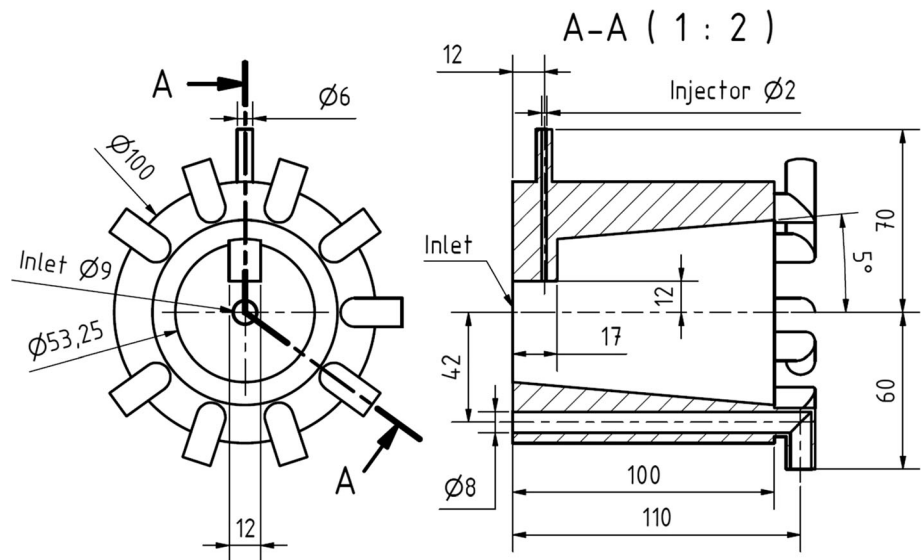


**Fig. 4** Technical drawing of the simulated nozzle extension



solid and fluid domains by facilitating the exchange of thermal energy at the interfaces between them. The conjugate heat transfer (CHT) method was used to analyze the heat transfer between the solid wall of the nozzle extension and the surrounding fluid domain. CHT can be modeled by coupling the fluid and solid domains using the heat transfer coefficients at the interface to consider both convection and conduction heat transfer (Ref 31). This allows for the simultaneous solution of the Navier–Stokes equations, the

energy equation, and the heat diffusion equation, providing a comprehensive analysis of the heat transfer process.

Conjugate heat transfer refers to the coupled analysis of heat transfer between fluids and solids. Addressing heat transfer in the solid shroud represents a CHT problem, as both heat conduction within the solid and convection in the fluid phase must be investigated. In solid domains, the conservation of energy equation can account for heat transport due to solid motion, conduction, and volumetric heat sources, as expressed by Eq 1 (Ref 32):

$$\frac{\partial(\rho h)}{\partial t} + \nabla \cdot (\rho U_s h) = \nabla \cdot (\lambda \nabla T) + S_E \tag{Eq 1}$$

where  $h$  is the enthalpy,  $\rho$  density, and  $\lambda$  the thermal conductivity of the solid,  $U_s$  is the solid velocity, if specified, and  $S_E$  is an optional volumetric heat source.

In our numerical model, where the solid shroud is motionless and does not have internal heat source, the previous equation simplifies to Eq 2:

$$\frac{\partial(\rho h)}{\partial t} = \nabla \cdot (\lambda \nabla T) \tag{Eq 2}$$

As the fluid domain incorporates initially solid-state injected particles, along with a mixture of gases, i.e., air in local thermodynamic equilibrium, argon, and aluminum oxide vapor, the fluid domain was modeled as a multiphase problem utilizing fluid pair models. Consequently, the heat transfer for the fluid domain is fluid-dependent. The convection part of heat transfer was modeled using the total energy equation derived from the fundamental Navier–Stokes equations. The numerical simulation employs the conservative interface flux condition for heat transfer at the interface between the solid shroud and the fluid domain. This condition ensures an accurate representation of the heat flux across the interface, conserving the overall balance of energy during the simulation. This is important for maintaining the accuracy and physical consistency of the simulation, especially when dealing with multiphase problems and CHT condition.

For modeling the particle–plasma interaction, the convective heat transfer  $Q_c$  depends on the difference between the plasma gas temperature  $T_g$  and the particle temperature  $T_p$ , interfacial area  $A_i$  as well as on the heat transfer coefficient  $h_c$  as expressed in Eq 3:

$$Q_c = h_c A_i (T_g - T_p) \tag{Eq 3}$$

The heat transfer coefficients in the model are not static but dynamic values incorporated through user routines in ANSYS CFX, and can be expressed using Eq 4:

$$h_c = \frac{\kappa_g \text{Nu}_p}{d_p} \tag{Eq 4}$$

where  $\kappa_g$  is the thermal conductivity of the plasma gas,  $\text{Nu}_p$  represents the particle Nusselt number, and  $d_p$  is the particle diameter.

Table 1 provides the process parameters used in this study. Simulations are conducted using the parameter set consisting of an argon flow rate of  $Q_{Ar} = 50$  SLPM and an electric current of  $I = 500$  A, while experimental measurements are conducted for the three different electrical currents  $I = 500, 450,$  and  $400$  A with the constant argon flow rate of  $Q_{Ar} = 50$  SLPM. In addition, simulations are

**Table 1** Process parameters for simulations and experiments

Parameter, [unit]	Value
Primary gas flow, Ar [SLPM]	50
Electric current, A	500, 450, 400
Carrier gas flow, SLPM	5
Powder feed rate, g/min	25
Particle size distribution, $\mu\text{m}$	– 45 + 22
Feedstock material	Alumina

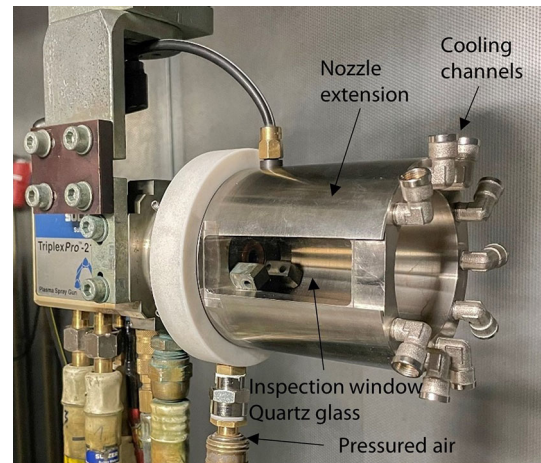


**Fig. 5** Installation of the constructed nozzle extension on the three-cathode plasma generator for experimental measurements

carried out without a nozzle extension to compare the behavior of the plasma jet to that of a conventional nozzle.

### Experimental Setup

The simulated solid shroud is constructed to conduct experiments on its impact on the plasma jet. Figure 5 shows the installation of the constructed nozzle extension on the three-cathode plasma generator for experimental measurements. For diagnostic measurements by a high-speed camera, the designed nozzle extension has an inspection window that is covered with a transparent quartz glass. The high-speed videography is conducted to describe the plasma intensities and its fluctuations with the nozzle extension and without it. The high-speed camera Fastcam SA-Z by Photron equipped with the macro-lens Irix 150 mm f/2.8 was positioned 500 mm away from the torch axis to take videos from the plasma jet. For this investigation, a frame rate of 100,000 fps was used, along with a shutter speed of 1.00  $\mu\text{s}$ . This allowed for a resolution of  $640 \times 280$  pixels, resulting in a field of view large enough to capture the entire length of the plasma jet. A neutral density filter (ND64) was used to decrease the intensity of

the recorded imaging and to prevent overexposure. During the videography measurements, the powder feeder was disabled.

Furthermore, to differentiate the possible impact of the solid shroud on the flow conditions within the plasma jet from the effects of power input fluctuations, current, and voltage measurements were conducted synchronized with the high-speed videography recordings. This approach allowed for ensuring a similar initial state with respect to power fluctuations, and thus for a reliable comparison of the measurements obtained without and with the nozzle extension. Measurements of the three voltages and three currents of the three-cathode plasma generator were carried out by the SIRIUS data capturing unit, manufactured by Dewesoft Company in Trbovlje, Slovenia. The sampling rate for the measurements was 500 kHz. The data acquisition device can measure voltage with a measurement uncertainty of  $\pm 2$  mV and current with  $\pm 5$  mA.

Moreover, two Type K thermocouple sensors connected to the data capturing unit were used to monitor the wall temperature of the nozzle extension. One sensor was placed at the beginning and the other at the end of the solid shroud. In addition, in-flight particle velocities and temperatures were experimentally measured at a spray distance of  $y = 150$  mm using the particle diagnostic system DPV-2000 manufactured by Tecnar Automation Ltd. in St. Bruno, QC, Canada. The DPV-2000 is a widely used diagnostic system in thermal spraying that employs the principle of two-wavelength pyrometry. Utilizing a local measurement technique, this system has a relatively small measurement volume of less than  $1 \text{ mm}^3$ . It examines the radiation intensities of particles at specific wavelengths and simplifies the particles as gray emitters. It is important to note that the DPV-2000 is designed to detect and measure only relatively hot particles. It is capable of analyzing the size, velocity, and temperature of these particles by capturing the radiation peaks generated when they pass through the measurement volume composed of a double slot mask in the measuring head. The detected signal is then transmitted to the detection unit via a fiber optic cable for further analysis. Please refer to (Ref 33) for further details on the measuring principle of this diagnostic device.

## Results and Discussion

This chapter begins with a presentation of the simulation results, which analyze the impact of the solid nozzle extension on the plasma flow and in-flight particle properties. Following this, the results of the voltage and current measurements synchronized with the high-speed videography are discussed.

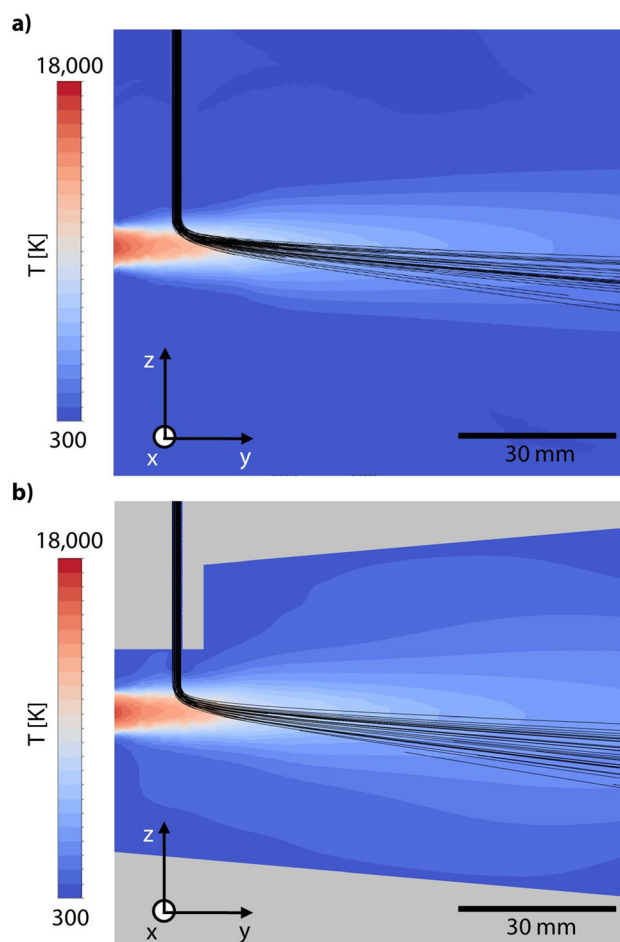


**Fig. 6** Distributions of gas temperature (a) without nozzle extension and (b) with nozzle extension

The simulation results of the plasma gas temperature and velocity for both the conventional nozzle and the solid nozzle extension cases are shown in Figs. 6 and 7, respectively. A part of the simulated particle trajectories is also depicted in black in both figures as an example. The process parameters for these simulations are given in Table 1 for an argon flow rate of  $\dot{Q}_{\text{Ar}} = 50$  SLPM and electric current of  $I = 500$  A. The results reveal that the nozzle extension has increased the temperature field compared to the conventional nozzle, and the plasma jet has been prolonged and enlarged in the presence of the solid shroud. Additionally, the solid shroud has resulted in an asymmetric temperature profile for the plasma gas, particularly near the shroud walls, compared to the case without nozzle extension. This suggests that the presence of the shroud influences the heat distribution and flow patterns of the plasma gas, causing variations in temperature distribution. However, the difference in gas velocity for the two nozzles is not significant. One possibility is that the design and dimensions of this nozzle extension are such



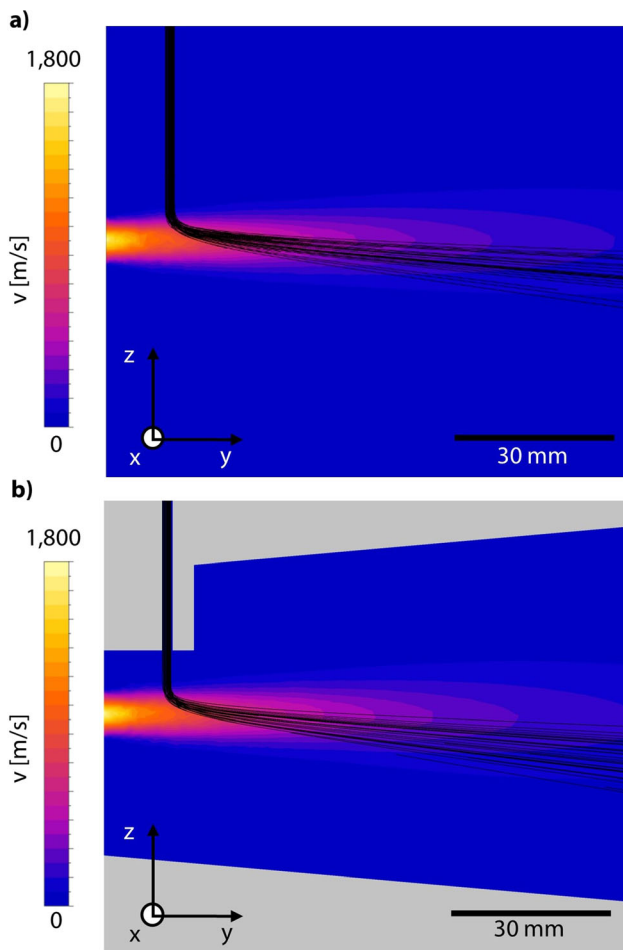


**Fig. 7** Distributions of gas velocity (a) without nozzle extension and (b) with nozzle extension

that they promote similar gas flow velocities as the case without a solid shroud.

The wall temperature of the solid shroud is an important factor that must be considered during shroud geometry design. To address this, the cooling channels were considered in the simulation model, and the CHT technique was used to analyze the convection and conduction heat transfer between the solid and fluid domain. The area-averaged wall temperature of the simulated solid shroud was calculated to be  $T_{w,sim} = 131.72\text{ }^{\circ}\text{C}$ . The corresponding mean temperature of the two thermocouple sensors on the shroud wall in the experimental setup was  $T_{w,exp} = 183.80\text{ }^{\circ}\text{C}$ , demonstrating a fair validation of the simulated heat transfer phenomena. Following that, the energy expended on cooling the shroud was calculated to be  $\dot{Q}_c = 41.38\text{ kW}$ . These results highlight the importance of considering the cooling channels and employing the CHT method in designing the solid shroud geometry to

prevent overheating and ensure the efficient operation of the plasma spraying process.

Figure 8 presents a comparison between the results of simulations and experiments for in-flight particle temperatures, (a) without and (b) with the nozzle extension, versus particle diameters. The data are sorted according to ascending particle diameters. The simulations and experiments in this figure were conducted at a spray distance of  $y = 150\text{ mm}$ , using an argon flow rate of  $\dot{Q}_{Ar} = 50\text{ SLPM}$  and an electric current of  $I = 500\text{ A}$ . Since the DPV can only give an estimate of the particle diameters, the measured diameters were rescaled to match the range of the diameters simulated in this study. To do this, a linear transformation was applied to match the mass-based mean values of the particle diameters. This effectively maps the experimental particle diameters to the simulation range while preserving the relative proportions between the diameters. This normalization procedure ensures that the measured diameters can be compared directly with the simulated ones. Due to the different particle size distributions, the arithmetically averaged particle properties cannot be compared. Therefore, the mass-based mean particle temperatures are determined using Eq 5. The mass-based mean values for simulations and experiments are also plotted in Fig. 8 as dashed and solid line, respectively.

$$\bar{T}_p = \frac{1}{M} \sum_{i=1}^{n_p} T_{p,i} m_{p,i} \tag{Eq 5}$$

$\bar{T}_p$  Mass-based mean particle temperature,  $T_{p,i}$  Temperature of particle  $i$ ,  $m_{p,i}$  Mass of the particle  $i$ ,  $n_p$  Number of particles,  $M$  Total mass of the particles

The simulation results of the particle temperatures in Fig. 8 show a notable increase when the nozzle extension is present. This trend is consistent with the experimental results. Additionally, it is evident that the simulated particle temperatures are closely approaching the vaporization limit of  $\text{Al}_2\text{O}_3$  in the presence of the nozzle extension ( $T_{\text{vapor}} = 3250\text{ K}$ ). Therefore, a significant portion of the particles in the simulations has completely melted, and some of their mass, particularly the smaller particles, has already evaporated. The measurements partially validate this outcome. However, when making a comparison, it is important to note that the simulated particle temperatures represent the average temperature of the particles, while the experimental measurements using the DPV can only determine surface temperatures.

Analogous to Eq 5 and Fig. 8, the mass-based mean particle velocities are calculated and plotted. Figure 9 shows these results for the simulations and the experimental measurements, both without and with the nozzle extension. The results presented in this figure are also obtained at a spray distance of  $y = 150\text{ mm}$ , using an argon

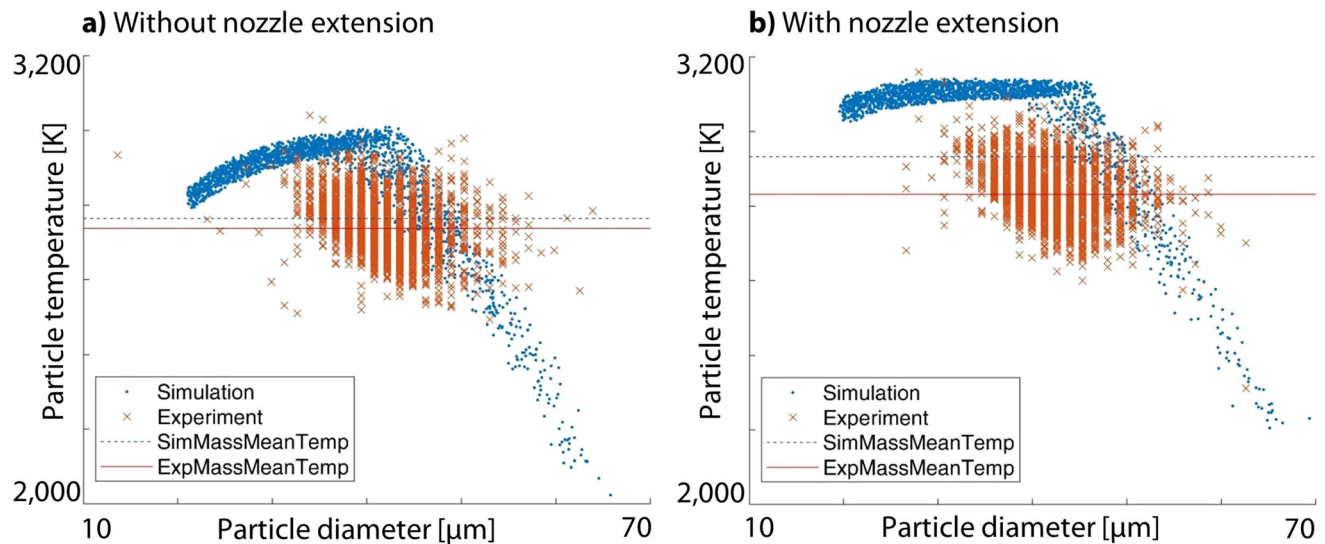


**Fig. 8** Comparison of simulations and experiments for in-flight particle temperatures (a) without and (b) with nozzle extension at a spray distance of  $y = 150$  mm for an argon flow rate of  $Q_{Ar} = 50$  SLPM and electric current of  $I = 500$  A

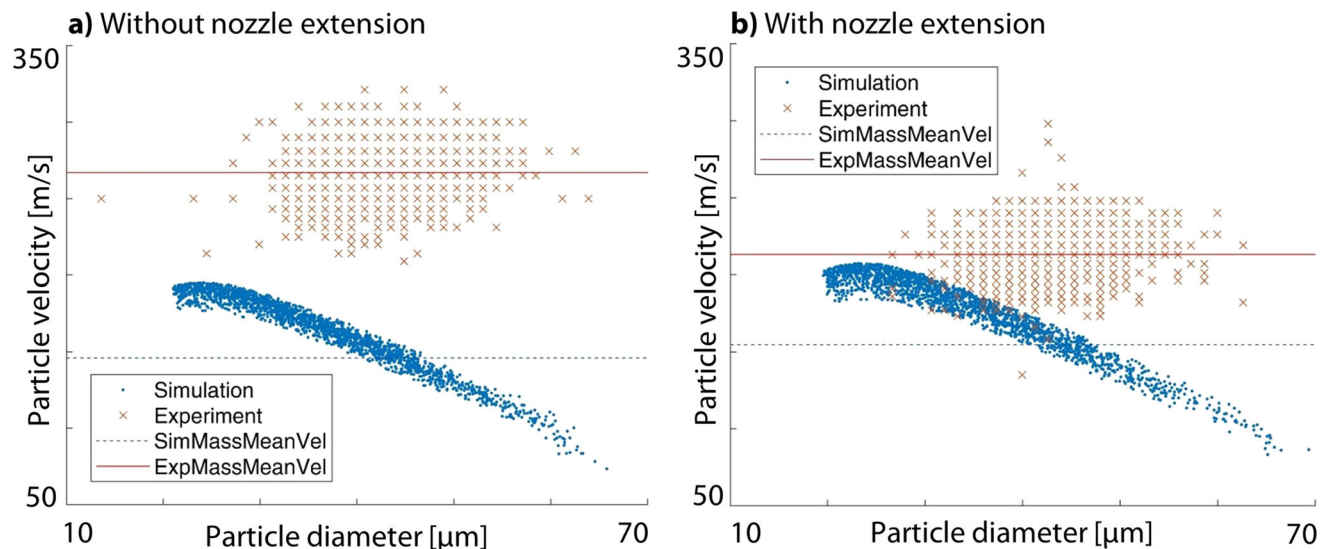


**Fig. 9** Comparison of simulations and experiments for in-flight particle velocities (a) without and (b) with nozzle extension at a spray distance of  $y = 150$  mm for an argon flow rate of  $Q_{Ar} = 50$  SLPM and electric current of  $I = 500$  A

flow rate of  $\dot{Q}_{Ar} = 50$  SLPM and an electric current of  $I = 500$  A. Directly evident is the underestimation of the particle velocities by the simulations. This could be attributed to the assumption used to calculate the drag coefficient between particles and gas, which depends, among other factors, on the Reynolds number and thus, on the particle size and temperature (Ref 29). The formulated relationships for the drag coefficient in the literature are given for spheres, and this assumption is not completely valid for angular and blocky particles. This should be considered in future simulations. The experimental results reveal a decrease in particle velocities with the use of the solid shroud. This phenomenon can be attributed to the

creation of a higher-pressure zone in the plasma jet, which causes gas drag and reduces the particle velocity. The high-pressure gas inside the shroud can also create recirculating flows or stagnation zone, further contributing to the reduction in particle velocity. However, the simulation results do not replicate this trend and show a minor increase in particle velocity. This discrepancy can be explained by considering the continuity equation for incompressible fluids, which is accounted for in the simulation. The fixed shroud narrows down the cross-sectional area of the flow compared to the case without nozzle extension, and according to the continuity equation, this

**Table 2** Root mean square (RMS) of voltages and total current for the case without and with the nozzle extension using the parameter set 50 SLPM-500 A

	RMS, unit			
	Voltage 1, V	Voltage 2, V	Voltage 3, V	Sum of currents, A
Without nozzle extension	91.81	91.32	92.50	497.55
With nozzle extension	91.94	91.30	92.55	498.48

should result in an increase in fluid velocity to maintain mass conservation.

The arc voltage is closely linked to factors such as arc current, torch geometry, gas flow rate, and gas composition as well as the flow characteristics of the plasma jet. The introduction of the solid shroud influences the flow properties within the shroud, leading to modifications in properties such as pressure and temperature. The gas dynamics and thermal effects caused by the shroud play an important role in this interaction and can subsequently affect the arc voltage. The possible influence of the solid shroud on the arc voltage was investigated using voltage and current measurements. These measurements were designed to isolate the effects of the input power fluctuations, focusing solely on understanding the effects of the developed shroud. The results of voltage and current measurements are presented below. As mentioned earlier, the three voltages between the three cathodes and one anode of the multi-arc plasma generator, together with their currents, were measured at a sample rate of 500 kHz. Root mean square (RMS) values of the voltages and the sum of currents were obtained for the case without and with the nozzle extension, using the parameter set of 50 SLPM-500 A. The results presented in Table 2 indicate only minor differences in values between both cases, suggesting a negligible influence of the solid shroud on the arc voltages. To better understand the relative stability of the three voltages of the plasma generator comparing both cases, the coefficient of variation (CV) was calculated for the measured data. The CV is a statistical measure defined as the ratio of the standard deviation to the mean and quantifies the degree of variation of a dataset around its mean. Figure 10 displays the CV values for the mean of the three voltages for different sets of process parameters for both without and with the nozzle extension. The findings demonstrate that the stability of the plasma arc for the conventional nozzle case and with the nozzle extension are nearly the same. This observation indicates that the initial state regarding the fluctuation of the power input was equivalent for both cases, and that the designed solid shroud does not exert any noticeable influence on the voltages of the plasma generator arcs. In other words, it is ensured that the fluctuation of the input power is isolated when analyzing the effect of the solid shroud on the plasma flow.

The transparent inspection window designed on the solid nozzle extension allows high-speed videography of the plasma jet. These recordings were synchronized with the aforementioned voltage and current measurements. This approach was intended to ensure the same initial conditions regarding power fluctuations when comparing flame intensities. Figure 11 presents the outcomes obtained from the high-speed videography of the plasma jet, considering both the cases without and with the nozzle extension, using different sets of process parameters. The corresponding videos of this figure are attached in the supplementary files. The results demonstrate that increasing the electrical current leads to an elongation of the plasma jet and an increase in its intensity. When comparing both cases for each set of process parameters, minimal differences can be observed in terms of the plasma form. This suggests that the designed nozzle extension does not appear to have a detrimental effect on the plasma form and maintains the overall plasma dynamics.

## Conclusions and Outlook

Plasma spraying is a flexible coating technology with challenges of high energy consumption and oxidation of metallic spray particles. Modified plasma spraying processes using a gas or solid shroud have been developed to address these challenges. While prior research mainly focused on single-cathode plasma generators, this study aimed to analyze the effects of a solid shroud as a nozzle extension on the plasma jet of a three-cathode plasma generator numerically and experimentally. A CFD model was developed to simulate a solid shroud with cooling channels analyzed with conjugate heat transfer method inside a simulation enclosure. The simulated design was then constructed for experimental analysis. The experimental setup included a nozzle extension with a transparent window for high-speed videography of the plasma jet and thermal sensors to monitor the wall temperature of the nozzle extension. Particle diagnostics were also conducted to analyze the properties of in-flight particles without and with the solid shroud. To isolate the effects of the solid shroud from fluctuations in the power input, current, and voltage measurements were carried out synchronized with the high-speed recordings. Based on the findings of this study, the following conclusions can be drawn:

**Fig. 10** Coefficient of variation of the mean voltages for different sets of parameters in case of the conventional nozzle and the nozzle extension

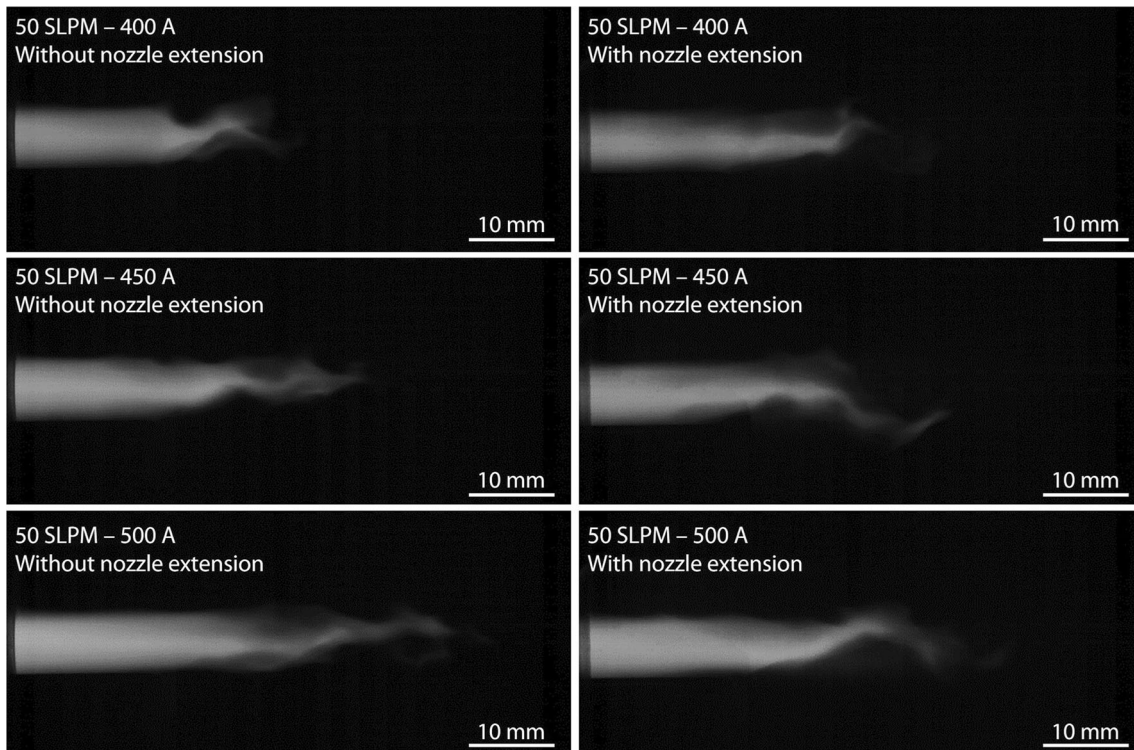
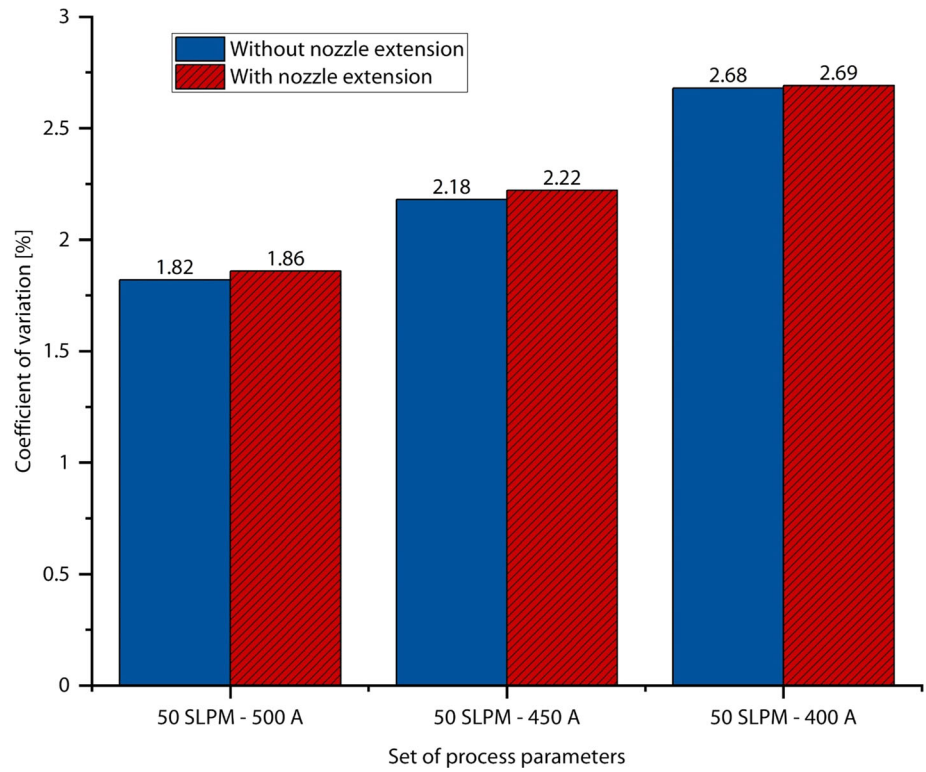


**Fig. 11** High-speed recordings of the plasma jet in case of without and with the nozzle extension for different sets of process parameters (videos are attached in the supplementary files)

- The designed solid shroud caused an increase in plasma temperature and prolonged the area of elevated temperatures compared to the conventional nozzle.
- No significant change was observed in plasma velocity in the presence of the solid shroud.
- The nozzle extension resulted in an increase in in-flight particle temperature and a decrease in in-flight particle velocity according to the experimental measurements.
- The voltage and current measurements indicated that the designed solid shroud had no impact on the voltage of the plasma arc, and the influence of input power fluctuations was isolated when analyzing the effect of the solid shroud on the plasma flow.

The calculated coefficients of variation for flame intensity resulting from the synchronized high-speed videography showed slightly more plasma fluctuation in the presence of the solid shroud for certain sets of process parameters. The optimal choice of shroud design and operating conditions must be carefully balanced to minimize plasma fluctuations.

In future work, the developed numerical model can be used to optimize the shroud geometry to adapt it to different flow conditions for various process parameters, and thus minimize plasma fluctuations. Moreover, the developed numerical model can be expanded to account for the oxidation and potential clogging of metallic particles. It can also be extended to incorporate a combination of argon and hydrogen as the plasma gas. Additionally, the coating properties should be analyzed to investigate the effect of the designed solid shroud on the microstructure of the coating.

**Supplementary Information** The online version contains supplementary material available at <https://doi.org/10.1007/s11666-024-01715-5>.

**Acknowledgments** This work was based on the DFG project BO 1979/79-1 with the project number 442323795 entitled “Increasing the energy efficiency of plasma spraying by means of simulation-based process development”. The authors gratefully acknowledge the financial support of the German Research Foundation (DFG). Simulations were performed with computing resources granted by RWTH Aachen University under the projects rwth0570 and rwth1204.

**Funding** Open Access funding enabled and organized by Projekt DEAL.

**Open Access** This article is licensed under a Creative Commons Attribution 4.0 International License, which permits use, sharing, adaptation, distribution and reproduction in any medium or format, as long as you give appropriate credit to the original author(s) and the source, provide a link to the Creative Commons licence, and indicate if changes were made. The images or other third party material in this article are included in the article’s

Creative Commons licence, unless indicated otherwise in a credit line to the material. If material is not included in the article’s Creative Commons licence and your intended use is not permitted by statutory regulation or exceeds the permitted use, you will need to obtain permission directly from the copyright holder. To view a copy of this licence, visit <http://creativecommons.org/licenses/by/4.0/>.

## References

1. P.L. Fauchais, J.V. Heberlein and M.I. Boulos, *Thermal Spray Fundamentals: From Powder to Part*, Springer, US, 2014.
2. J.R. Fincke, W.D. Swank and D.C. Haggard, Plasma Spraying of Alumina: Plasma and Particle Flow Fields, *Plasma Chem. Plasma Process.*, 1993, **13**(4), p 579–600.
3. K. Taheri, M. Elhoriny, M. Plachetta and R. Gadow, Thermodynamic Analysis of Resources Used in Thermal Spray Processes: Energy and Exergy Methods, *Entropy*, 2016, **18**(7), p 237.
4. M.L. Thorpe, Thermal Spray Industry in Transition, *Adv. Mater. Processes*, 1993, **143**(5), p 50–56.
5. K. Wen, X. Liu, M. Liu, K. Zhou, H. Long, C. Deng, J. Mao, X. Yan and H. Liao, Numerical Simulation and Experimental Study of Ar-H<sub>2</sub> Dc Atmospheric Plasma Spraying, *Surf. Coat. Technol.*, 2019, **371**, p 312–321.
6. K. Bobzin, M. Öte, J. Schein, S. Zimmermann, K. Möhwald and C. Lummer, Modelling the Plasma Jet in Multi-arc Plasma Spraying, *J. Therm. Spray Technol.*, 2016, **25**(6), p 1111–1126.
7. E. Pfender, J. Fincke and R. Spores, Entrainment of Cold Gas into Thermal Plasma Jets, *Plasma Chem. Plasma Process.*, 1991, **11**(4), p 529–543.
8. P. Roumilhac, J.F. Coudert, and P. Fauchais, Influence of the Arc Chamber Design and of the Surrounding Atmosphere on the Characteristics and Temperature Distributions of Ar-H<sub>2</sub> and Ar-He Spraying Plasma Jets, in *MRS Proc.*, 190 (1990)
9. S. Shankar, D.E. Koenig and L.E. Dardi, Vacuum Plasma Sprayed Metallic Coatings, *JOM*, 1981, **33**(10), p 13–20.
10. B.J. Gill and R.C. Tucker, Plasma Spray Coating Processes, *Mater. Sci. Technol.*, 1986, **2**(3), p 207–213.
11. L. Zhao and E. Lugscheider, Influence of the Spraying Processes on the Properties of 316L Stainless Steel Coatings, *Surf. Coat. Technol.*, 2003, **162**(1), p 6–10.
12. I. Thomson, V. Pershin, J. Mostaghimi and S. Chandra, Experimental Testing of a Curvilinear Gas Shroud Nozzle For Improved Plasma Spraying, *Plasma Chem. Plasma Process.*, 2001, **21**(1), p 65–82.
13. M.P. Planche, H. Liao and C. Coddet, Oxidation Control in Atmospheric Plasma Spraying Coating, *Surf. Coat. Technol.*, 2007, **202**(1), p 69–76.
14. M.F. Morks and C.C. Berndt, Corrosion and Oxidation Properties of NiCr Coatings Sprayed in Presence of Gas Shroud System, *Appl. Surf. Sci.*, 2010, **256**(13), p 4322–4327.
15. G. Espie, A. Denoirjean, P. Fauchais, J.C. Labbe, J. Dubsky, O. Schneeweiss and K. Volenik, In-Flight Oxidation of Iron Particles Sprayed Using Gas and Water Stabilized Plasma Torch, *Surf. Coat. Technol.*, 2005, **195**(1), p 17–28.
16. G. Espie, P. Fauchais, B. Hannover, J.C. Labbe and A. Vardelle, Effect of metal particles oxidation during the aps on the wettability, *Ann. New York Acad. Sci.*, 1999, **891**(1), p 143–151.
17. H. Zhang, A. Vardelle and N.J. Themelis, In-Flight Oxidation and Evaporation of Plasma-Sprayed Iron Particles, *High Temp. Mat. Proc.*, 2003, **7**(3), p 277–298.

18. T. Liu, L. Zheng and H. Zhang, Effect of Solid Shield on Coating Properties in Atmospheric Plasma Spray Process, *J. Therm. Spray Technol.*, 2016, **25**(8), p 1502–1515.
19. S. Matthews, Shrouded Plasma Spray of Ni–20Cr Coatings Utilizing Internal Shroud Film Cooling, *Surf. Coat. Technol.*, 2014, **249**, p 56–74.
20. J. Kim, K. Kang, S. Yoon and C. Lee, Enhancement of Metallic Glass Properties of Cu-Based Bmg Coating by Shroud Plasma Spraying, *Surf. Coat. Technol.*, 2011, **205**(8–9), p 3020–3026.
21. D.T. Gawne, T. Zhang and B. Liu, Computational Analysis of the Influence of a Substrate, Solid Shield and Gas Shroud on the Flow Field of a Plasma Jet, *Surf. Coat. Technol.*, 2002, **153**(2–3), p 138–147.
22. M. Jankovic and J. Mostaghimi, A New Nozzle Design For Dc Plasma Spray Guns, *Plasma Chem. Plasma Process.*, 1995, **15**(4), p 607–628.
23. M. Jankovic, J. Mostaghimi and V. Pershin, Design of a New Nozzle For Direct Current Plasma Guns With Improved Spraying Parameters, *J. Therm. Spray Technol.*, 2000, **9**(1), p 114–120.
24. H.-X. Wang, X. Chen and W. Pan, Effects of the Length of a Cylindrical Solid Shield on the Entrainment of Ambient Air into Turbulent and Laminar Impinging Argon Plasma Jets, *Plasma Chem. Plasma Process.*, 2008, **28**(1), p 85–105.
25. A. Dolatabadi, J. Mostaghimi and V. Pershin, Effect of a Cylindrical Shroud on Particle Conditions in High Velocity Oxy-Fuel Spray Process, *Sci. Technol. Adv. Mater.*, 2002, **3**(3), p 245–255.
26. K. Bobzin and M. Öte, Modeling Multi-Arc Spraying Systems, *J. Therm. Spray Technol.*, 2016, **25**(5), p 920–932.
27. K. Bobzin, H. Heinemann and S.R. Dokhanchi, Numerical Investigation of the Effect of a Nozzle Extension on the Plasma Jet in Multi-Arc Plasma Spraying, *J. Therm. Spray Technol.*, 2023 <https://doi.org/10.1007/s11666-023-01588-0>
28. K. Bobzin, M. Öte, J. Schein and S. Zimmermann, Numerical Study on Plasma Jet and Particle Behavior in Multi-Arc Plasma Spraying, *J. Therm. Spray Technol.*, 2017, **26**(5), p 811–830.
29. K. Bobzin and M. Öte, Modeling Plasma-Particle Interaction in Multi-Arc Plasma Spraying, *J. Therm. Spray Technol.*, 2017, **26**(3), p 279–291.
30. A. Burcat, B. Ruscic, and Chemistry, Third millenium ideal gas and condensed phase thermochemical database for combustion (with update from active thermochemical tables). 2005.
31. M. Silieti, A.J. Kassab and E. Divo, Film Cooling Effectiveness: Comparison of Adiabatic and Conjugate Heat Transfer Cfd Models, *Int. J. Therm. Sci.*, 2009, **48**(12), p 2237–2248.
32. ANSYS CFX-Solver, Theory Guide, ANSYS, Inc. and ANSYS Europe, Ltd., 2020.
33. G. Mauer, R. Vaßen and D. Stöver, Plasma and Particle Temperature Measurements in Thermal Spray: Approaches and Applications, *J Therm Spray Tech*, 2011, **20**(3), p 391–406.

**Publisher's Note** Springer Nature remains neutral with regard to jurisdictional claims in published maps and institutional affiliations.